ACS SENSORS

pubs.acs.org/acssensors

Article

Combination of Live Cell Surface-Enhanced Raman Scattering Imaging with Chemometrics to Study Intracellular Nanoparticle Dynamics

Elisa Lenzi, Malou Henriksen-Lacey, Beatriz Molina, Judith Langer, Carlos D. L. de Albuquerque, Dorleta Jimenez de Aberasturi,* and Luis M. Liz-Marzán*

Cite This: *ACS Sens.* 2022, 7, 1747−1756

Read Online

ACCESS | Metrics & More | Article Recommendations | Supporting Information

ABSTRACT: Surface-enhanced Raman scattering (SERS)-encoded nanoparticles are used for bioimaging, on account of their well-defined Raman spectra and biocompatibility, which allow long incubation times with high signal stability and no cytotoxicity. However, reliable analysis of SERS bioimaging requires quantification of the amount of encoded nanoparticles that have been taken up by cells and the effect of subsequent dilution due to cellular division (mitosis). Although methods such as elemental analysis and flow cytometry can be used to quantify nanoparticle uptake, these are both end-point measurements in which a cell population is screened rather than looking at individual cells. In contrast, SERS imaging can be applied at multiple timepoints to the same individual cells without damaging the biological sample. We present the application of both supervised and unsupervised multivariate analyses, to quantify the intracellular amount of SERS tags in individual MCF7 living cells, toward the characterization of cellular uptake *in vitro*. The obtained results from both methodologies were validated by standard elemental analysis techniques.

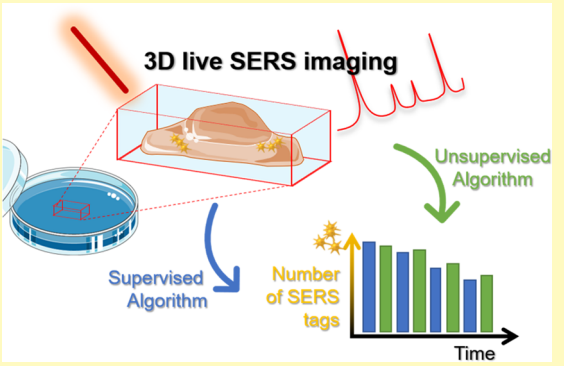

KEYWORDS: *SERS tags, SERS bioimaging, multivariate analysis, multiple linear regression analysis, non-negative matrix factorization analysis*

Synthesis and characterization of gold nanoparticles (AuNPs) are sufficiently mature to fully validate their use in bioimaging and biosensing.[1−7] Surface-enhanced Raman scattering (SERS) microscopy, in particular, combines the high sensitivity and multiplexing character of Raman fingerprints from molecules bound to AuNPs (collectively known as a SERS tags), with the excellent spatial resolution of new-generation confocal Raman microscopes. SERS tags can be used as nontoxic cell labeling moieties or as indirect sensors to detect the presence of biomolecules.[8−12] One of the benefits of SERS microscopy over, for example, fluorescence microscopy, is the absence of label bleaching, minimized spectral overlap, and reduced light-induced cytotoxicity, which may occur upon repeated irradiation in confocal fluorescence microscopy.[13] These features, together with the potential for multiplexing, provide the ability to image multiple labels simultaneously with a single irradiation laser, and over long periods of time.[14,15] However, SERS microscopy and especially confocal SERS microscopy of three-dimensional (3D) cell models, still suffer from long acquisition times, which make repetitive measurements over short timepoints complicated. Furthermore, when considering the motile nature of living cells, experimental setups must be optimized to accurately detect SERS tags *in situ*. It is well known that both NP uptake[16,17] and distribution of NPs during cellular division[18] are asymmetric random processes. Although the associated dilution of NPs into daughter cells can be influenced by exocytosis,[19] this is not the main mechanism.[20] The asymmetric nature of NP dilution into daughter cells is assumed to stem from the inhomogeneous distribution of intracellular vesicles in which the NPs are located. Delivery of NPs directly to the cytoplasm has been shown to improve the symmetry of NP distribution to daughter cells.[21] Unfortunately, the methods currently used to quantify NPs inside cells, such as inductively coupled plasma-mass spectrometry (ICP-MS) or flow cytometry, are destructive and, therefore, cannot always translate the biological processes into their real environment. Moreover, such techniques refer to the entire population of cells, whereas no studies regarding single live cells are available.[22] Therefore, a method is required which can both monitor and estimate the

Received: March 22, 2022
Accepted: May 26, 2022
Published: June 7, 2022

https://doi.org/10.1021/acssensors.2c00610
ACS Sens. 2022, 7, 1747−1756

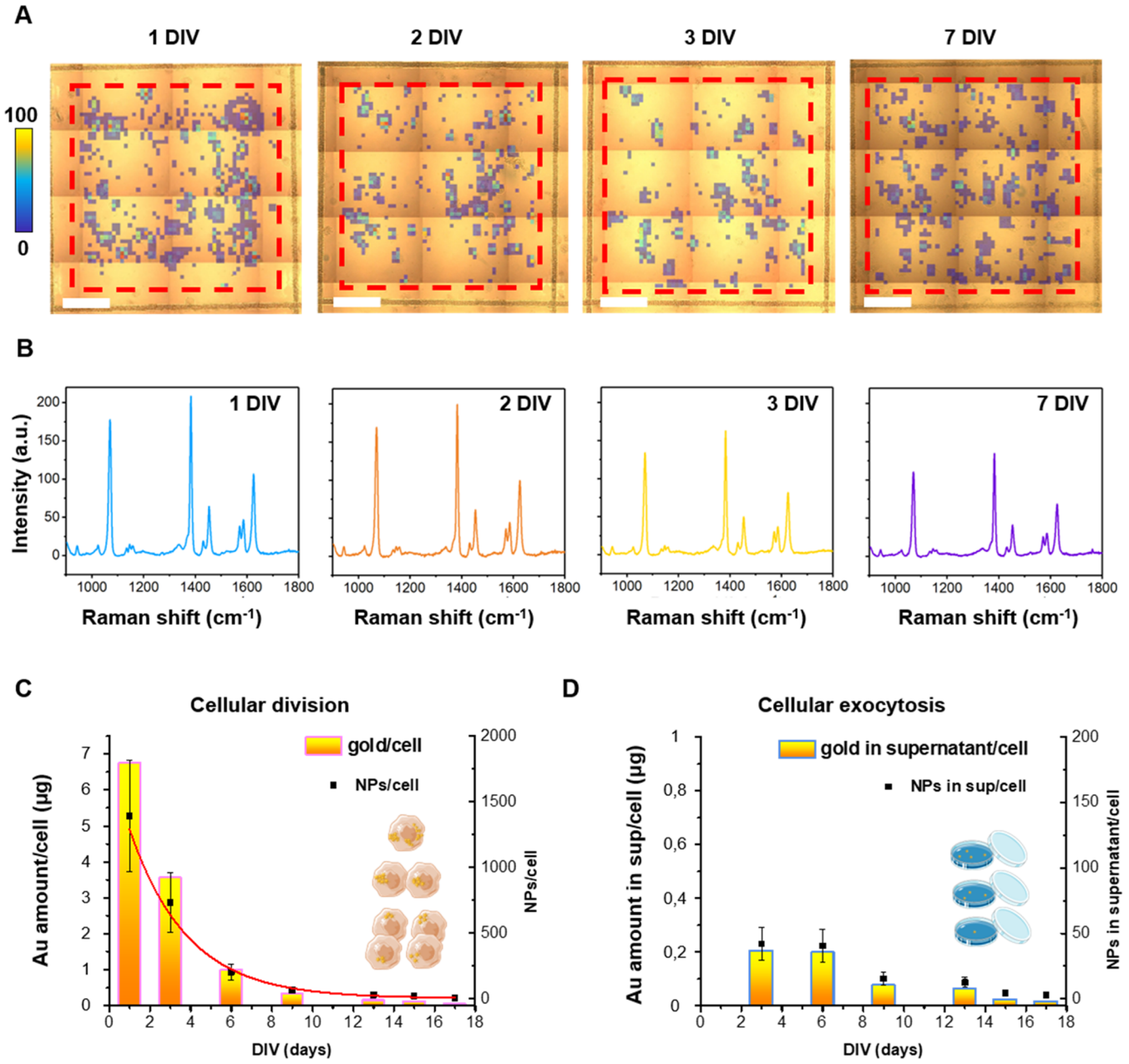

Figure 1. (A, B) Experimental data from 2D SERS maps of MCF7 cells labeled with SERS tags. (A) Merged bright-field and SERS maps showing only the selected points from those SERS maps matching the reference spectrum, obtained on days 1, 2, 3, and 7 post-seeding (red dashed squares indicate the boundary of the analyzed area). 2NAT-AuNR SERS tags were employed. Scale bars: 200 μm. (B) Averaged SERS spectra for 2NAT-AuNR SERS tags in the zone marked by the red dashed square in (A), showing a decrease in the average intensity over time. (C, D) Amount of Au per cell, obtained as the ratio between ICP-MS data and the corresponding number of cells in the sample. (C) Amount of gold inside cells (left axis) and relative number of NPs per cell (right axis), both showing a decreasing trend. The observed reduction is in good agreement (R^2 = 0.89) with an exponential function characterized by a half-life time of $\tau = 1/t_1$ = 2.2 days, which is consistent with the cellular division time of the MCF7 cell line. 4BPT-AuNS SERS tags were employed. (D) Exocytosed NPs, presented as Au amount (left axis) and number of NPs (right axis) detected in the supernatant and correlated to the total number of cells present in the sample. 4BPT-AuNS SERS tags were employed.

number of NPs in a complex biological environment while remaining minimally invasive.

To address these issues, we present herein a combination of SERS mapping with multivariate data analysis methods to study the dynamics of SERS NPs in a population of human breast cancer MCF7 cells. MCF7 cells express many of the physical and morphological properties required for confocal SERS imaging. These include adherence (enabling a fixed focal plane), immortalization (permitting changes in NP intensity to be studied in the same population over long periods of time), compact size and low aspect ratio (allowing multiple measurements on single cells to be carried out within an imaging window), division time of ca. 30 h (hence cells pre- and post-division can be studied within days), active endocytosis (allowing high levels of SERS tags to be internalized), and finally the ability to withstand high levels of confluence without contact inhibition (so the same imaging area can be continually studied without cells detaching from the surface). Regarding the SERS tags themselves, we used anisotropic AuNPs, namely, gold nanostars (AuNSs) and gold

https://doi.org/10.1021/acssensors.2c00610
ACS Sens. 2022, 7, 1747−1756

nanorods (AuNRs), coated with the Raman active molecules 4-biphenylthiol (4BPT) and 2-naphthalenethiol (2NAT), respectively, as previously reported (see the Materials and Methods section for synthesis details).[8] The selected NPs displayed localized surface plasmon resonances (LSPR) at ca. 780 nm, in resonance with the typically used 785 nm laser—within the first biological transparency window.[8] We have previously demonstrated that similar polymer-coated SERS tags are highly stable in *in vitro* environments, thanks to the colloidal stability imparted by the polymeric outer coating, which helps prevent AuNP aggregation, even in oxidizing environments.[10] On the basis of a previously reported method for the correlation of SERS tag intensities with the number of labeled AuNPs in a given area (SERSTEM),[23] we demonstrate herein the applicability of this method in biological samples by characterizing cellular uptake of SERS tags. Considering the biologically complex microenvironment within *in vitro* samples, it is crucial to correctly extract the signal of the SERS tags from the background, i.e., media, cell proteins, cell metabolites, etc.[24] To tackle this issue, we applied two multivariate analysis approaches: (1) A data-driven supervised algorithm (SA), based on multiple linear regression (MLR) analysis,[25−27] in which the output was compared to a reference spectrum from the SERS tags in solution, and (2) a digital unsupervised algorithm (DUA), based on non-negative matrix factorization (NMF) analysis,[28] which can be applied in those cases where a reference spectrum is not available.[29] The SA approach used MLR analysis to obtain the SERS intensity recorded from a single cell containing SERS tags. The average SERS signal of a labeled cell was analyzed by SERSTEM, to retrieve the number of uptaken SERS tags. The DUA used NMF to extract the number of spots in a single cell displaying the spectra corresponding to SERS tags (called SERS events), rather than SERS intensities.[30] The average number of SERS events was subsequently used to quantify the number of SERS tags in an individual cell, by means of a calibration curve derived from ICP-MS analysis. Both methods were compared and validated against each other, yielding similar results. Our findings suggest that SERS imaging coupled with multivariate data analysis can be used to estimate the number of AuNPs within single living cells, thereby offering an alternative, nondestructive method to determine NP uptake and subsequent partitioning into daughter cells.

RESULTS AND DISCUSSION

Supervised Analysis for SERS Tag Quantification. We modeled SERS uptake and subsequent cell division using simulated maps of SERS-labeled cells, analyzing them with an algorithm based on the MLR method, herein termed supervised algorithm (SA). Only those pixels inside the map whose SERS spectra match the reference spectrum of the selected SERS tags, with statistical significance, were analyzed. This selection was then used to calculate the descriptive parameters of the SA, and in turn the number of SERS tags inside the map area (see Table S1). We observed that the relative SERS intensity per unit area (**R**), which is the product of the total number of selected SERS spectra inside that area (surface coverage, $\boldsymbol{\sigma}$) times the average SERS signal per point (average intensity at a wavenumber $\tilde{\nu}$, $\overline{\mathbf{I}}_{\tilde{\nu}}$), is constant for maps containing the same number of SERS tags (Figure S1). Assuming that SERS tags do not leave the imaging area, on applying the SA to the same map but at a different timepoint, we would expect that **R** remains constant because the overall number of SERS tags within the cellular populations studied remains the same. This would be explained as a contemporary increase of $\boldsymbol{\sigma}$ and decrease of $\overline{\mathbf{I}}_{\tilde{\nu}}$, due to the dilution of SERS tags to daughter cells upon cellular division. Thus, we proceeded to apply this SA to experimental data obtained from SERS maps of MCF7 cells labeled with SERS tags (added at $[Au^0]$ = 0.1 mM, corresponding to 3.8×10^9 NPs/mL). As expected, we observed a reduction in the intensity and surface coverage of SERS tags over time (Figure 1A,B), which corresponds to a reduction in the number of SERS tags per cell, and their partitioning into daughter cells. Looking in detail at the number of cells at each timepoint we noted that, with the exception of DIV3, the number of cells in the imaging area (red dashed square in Figure 1A) was increased. The result observed at DIV3 (a decrease in cell number coupled with a decrease in SERS tag coverage), can only suggest that MCF7 cells migrated from the imaged area during the studied time window (Figure S2). This is a flaw of the analytical method, which we address below (see the Application of Supervised Analysis to 3D Images section).

SERS Tags Determination via ICP-MS. We thus quantified the gold concentration in MCF7 cells incubated with low SERS tag concentrations via ICP-MS, mimicking the expected SERS tag concentrations after successive cell divisions (see Figure S3). Specifically, we analyzed the possible range (30−0.04 μM, corresponding to ca. 3.8×10^9−1×10^6 NPs/mL) that would be expected after 17 days *in vitro* (DIV), based on the MCF7 doubling time and the previously used initial SERS tags concentration (3.8×10^9 NPs/mL). The results, determined via ICP-MS, show the possibility of detecting the equivalent to 1 NP/cell in a representative sample of 200 μL, containing 2×10^4 cells.

Cellular Division and Exocytosis. The decrease in the number of NPs inside cells can be related to several processes (see above). Hence, we addressed the possibility that the decrease in SERS intensity over time may be due to cellular exocytosis, i.e., the process by which cells secret substances to the outside, including SERS tags, in potential competition with cellular division (mitosis). We therefore investigated the amount of gold inside cells and in cell media over time, by means of ICP-MS. MCF7 cells were incubated with SERS tags (3.8×10^9 NPs/mL) for 24 h, followed by the removal of nonendocytosed NPs. According to ICP-MS analysis, ∼57% of the added tags were internalized after 24 h. We subsequently collected both cell and supernatant samples at various timepoints, to measure the amount of SERS tags that were transmitted to daughter cells via mitosis and those that were exocytosed, respectively. As can be seen in Figure 1C, the results confirmed that the reduction in the number of NPs inside cells followed an exponential function (with R^2 = 0.94) characterized by a half-life time of τ = 2.2 days, in agreement with the cellular division time of the MCF7 cell line.[31] With regards to the SERS tags released by exocytosis, once the nonendocytosed material was removed, we observed that the number of SERS tags found in the supernatant was negligible and accounted for less than 3% of the initially endocytosed material (Figure 1D). Our findings therefore suggest that the role of exocytosis in the decrease of SERS tag signal from cells is negligible and those SERS tags that were transmitted to daughter cells retained their initial (strong) SERS signal, thanks to the biocompatibility and high stability provided by the protective polymeric shell. Indeed, TEM imaging of MCF7 cells incubated with SERS tags confirms their uptake into

https://doi.org/10.1021/acssensors.2c00610
ACS Sens. 2022, 7, 1747−1756

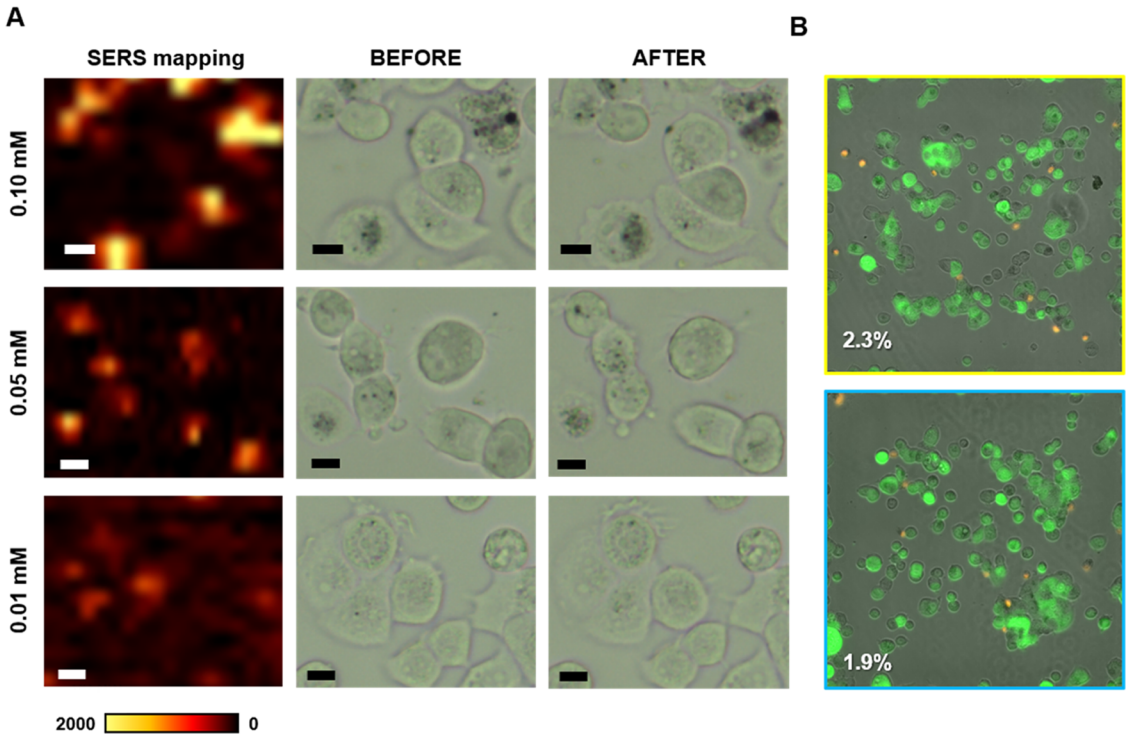

Figure 2. (A) SERS maps of MCF7 cells labeled with different SERS tag concentrations, imaged with a 785 nm laser at 5 mW (1.6 mW μm^{-2}) for 20 ms, and optical images before and after irradiation. Scale bars =10 μm. 4BPT-AuNS SERS tags were employed. (B) Optical images of SERS-labeled MCF7 cells with [Au^0] = 0.1 mM, in irradiated (5 mW laser power, 1.6 mW μm^{-2} power density, 20 ms accumulation time; top panel) and nonirradiated (bottom panel) areas. Fluorescence maps from live (green) and propidium iodide containing dead cells (red) were overlapped to the optical images. The percentage of dead cells (indicated in each image) was calculated as the ratio between red and green areas.

intracellular vesicles and the protective nature of the polymeric shell in preserving NS morphology in the intracellular environment (Figure S4).

Optimization of SERS Measurement Parameters. To obtain more accurate information on the number of SERS tags in an individual cell, the entire cell volume must be taken into consideration because the intracellular distribution of NPs is not homogeneous. However, realization of multiple scans at different z-depths often requires an increase in the laser energy delivered, which can have detrimental effects against cells. We thus investigated the risk of laser-induced (photo)toxicity and the minimum laser power required to obtain a meaningful SERS signal. These control experiments were carried out using laser powers ranging from 3 to 20 mW (equivalent to power densities ranging from 1.0 to 6.4 mW μm^{-2}), in combination with a 20× objective lens, for measurement of SERS maps in confocal mode. As expected, increasing the laser power resulted in an increase of the recorded SERS intensity (Figure S5A), which at high laser powers with continual irradiation resulted in extensive cell death, as confirmed by the appearance of apoptotic-like bodies and cell shrinkage (Figure S5B,C). Such an excessive cell death is attributed to plasmonic heating of AuNPs featuring an LSPR that accurately matched the irradiation laser wavelength. Indeed, MCF7 cells can tolerate much higher laser powers (80 mW, or 25.6 mW μm^{-2}) in the absence of SERS tags, without any apparent cytotoxic effects (Figure S6). We therefore aimed at identifying a sweet spot balancing SERS tag concentration and laser power, so that sufficient signal from SERS tags could be obtained while avoiding phototoxicity. We explored lower doses of SERS tags, coupled with a laser power of 5 mW (1.6 mW μm^{-2}), and making sure that the SERS signal intensity was maintained above the limit of detection (Figure 2A). The bright-field images obtained pre- and post-SERS imaging show that cells retained their morphology, and fluorescence live/dead assays (Figure 2B) verified their viability post-irradiation. The percentage of dead cells showed similar values in both irradiated (2.3%) and nonirradiated areas (1.9%), indicating that no phototoxicity effects were generated in SERS-labeled cells with [Au^0] = 0.1 mM (3.8×10^9 NPs/mL) and measurement parameters of 5 mW laser power (1.6 mW μm^{-2}) and 20 ms irradiation time. We thus selected these conditions for subsequent measurements. Furthermore, these conditions allowed us to reduce the scanning step size (in the *xy* axis) from 5 to 1 μm, thereby achieving a significantly improved SERS map resolution, yet avoiding laser-induced cytotoxic effects (Figure S7).

Application of Supervised Analysis to 3D Images. After identifying the optimal experimental conditions, including parameters such as step size, laser power, and SERS tag concentration, we proceeded to quantify the distribution of SERS tags over multiple z-planes, to obtain a representative NP/cell value for the whole 3D cellular volume. We implemented the previously described SA, by summing up the SERS intensity signals derived from multiple xy images at different z-heights, to obtain the overall signal from the cellular volume (see the Materials and Methods section for more details). Rather than using the imaging area as a descriptive parameter for the analysis, we established the number of cells to be imaged, which allowed us to conduct a more accurate analysis disregarding those cells that migrated away from the imaging field (imaging parameters are provided in Table S2). Considering that living cells were used, slightly different experimental conditions and calibration procedures were

https://doi.org/10.1021/acssensors.2c00610
ACS Sens. 2022, 7, 1747−1756

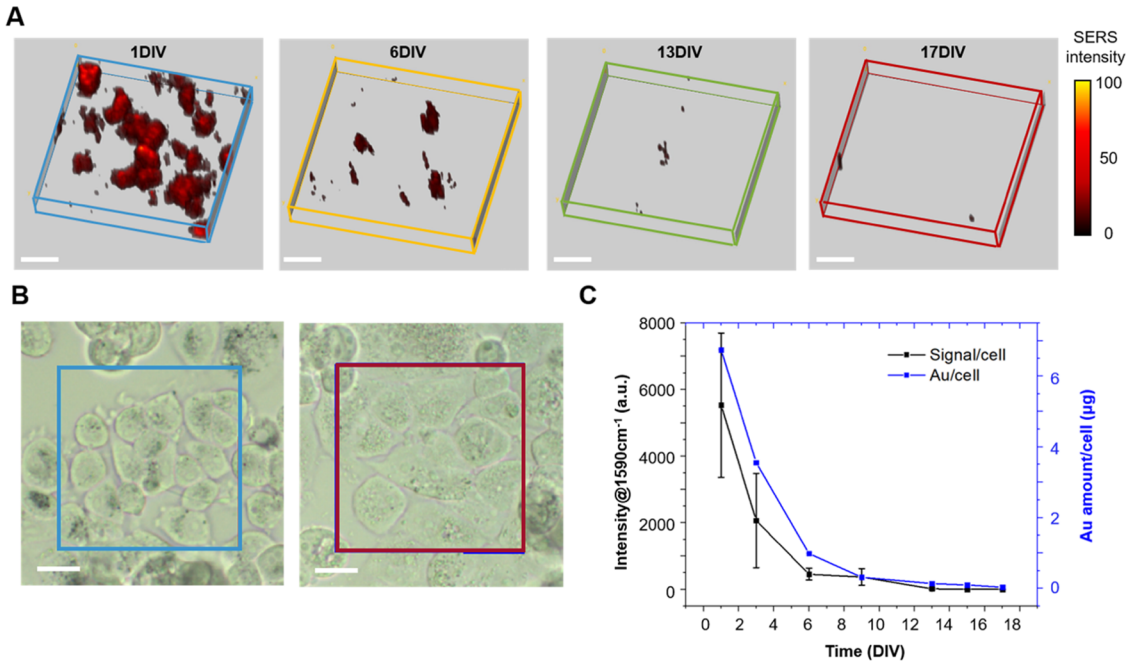

Figure 3. SERS analysis by SA. (A) 3D reconstructions of the selected SERS signal at four timepoints: 1 DIV, 6 DIV, 13 DIV, and 17 DIV. Colored boxes measure ca. 84 × 84 × 25 μm^3. 4BPT-AuNS SERS tags were employed. (B) Images corresponding to the 1 and 17 DIV, showing labeled cells in the measured areas. Optical images were used to count the cells and subsequently calculate the SERS signal per cell (see Figure S11). Scale bars = 20 μm. (C) Comparison between the average SERS intensity per cell (I_c) and the amount of gold (μg) per cell obtained via ICP-MS. Error bars indicate the standard deviations of ca. 30−80 SERS spectra recorded from single cells for SERS and triplicate measurements for ICP-MS.

required at the different timepoints (Figures S8 and S9). To provide a realistic comparison, two different SERS tag concentrations, [Au^0] = 0.1 and 0.05 mM (3.8 × 10^9 and 1.9 × 10^9 NPs/mL, respectively), were added to cells. Every 2−3 days for a period of 17 days, we imaged 3−4 volumetric areas, each containing between 10 and 20 cells, resulting in a total of between 30 and 80 cells per DIV (Figure 3). Using the SA procedure on the acquired 3D SERS images, we estimated the number of SERS tags per cell at each DIV and compared the results with the corresponding measurements obtained by ICP-MS analysis. As expected, a decrease in the average intensity of the SERS signal per cell (see Figure S10A,B) and a variation in the spatial distribution of the SERS signal over time (Figure 3A), were detected. For comparison, images showing the cell distribution on the first and last DIV are shown in Figures 3B and S11. In general, for each measured area of 84 × 84 μm^2, we preselected between 10 and 20 cells. We then compared the amount of gold per cell (determined by ICP-MS) with the average SERS signal intensity (at 1590 cm^{-1}) per cell, at each DIV (Figure 3C). The results are in excellent agreement, showing a decrease over time as previously predicted by the simulations. We observe a higher deviation in SERS measurements, compared to ICP-MS, because SERS measurements were performed on individual cells and not on the whole population. This deviation is due to the inhomogeneity in SERS tag uptake by cells, which may occur due to differences in cell size[32] (as a direct result of the cell cycle at that particular moment in time), or variations in NP sedimentation rate,[33] in agreement with previously reported simulations[34] and experimental results.[17] In contrast, ICP-MS measures Au in a bulk sample and the value is then correlated to the number of cells in the sample, counted using manual methods (i.e., a hemocytometer). The SA thus allowed us to monitor NP dilution in cells due to cellular mitosis, over nearly 2 weeks. We observed that, at the latest three timepoints, SERS imaging underestimated SERS tag uptake, as compared to ICP-MS data (Figure S10C). This can be explained by the low SERS signal in cells at such late timepoints. However, the estimation obtained by SERS is comparable to the experimental errors obtained by ICP-MS, indicating that this strategy may be suitable as an alternative, noninvasive, and fast method for the quantification of NPs in live cells. Indeed, similar results were also obtained for cells incubated with a lower concentration (0.05 mM, or 1.9 × 10^9 NPs/mL) of SERS tags (Figure S12). To better resolve the differences observed at late timepoints (13 DIV onwards), we adjusted the laser power to improve SERS tag detection, taking into consideration that the number of NPs per cell is considerably lower than that on DIV 1, and hence negligible laser-induced cytotoxicity is expected. As can be seen in Figure S13, such technical adjustments did allow us to better resolve the differences in SERS tag numbers at low concentrations.

Digital Unsupervised Algorithm for Quantification of SERS Tags. To refine the large variations in SERS tag intensities shown in Figure 3C, we explored a SERS tag quantification algorithm comprising a digital SERS tag calibration curve with extended linear range and precision.[30] In contrast to the SA, this digital unsupervised algorithm (DUA) estimates the abundance of NPs inside cells, thereby improving their identification at low SERS tag concentrations (workflows of the two techniques are shown in Figure S14). It has been reported that multivariate analysis, e.g., using non-negative matrix factorization (NMF) methods, can successfully recover the full SERS profile, with no need for providing prior information about the reference spectrum and even in the presence of potential interferences.[29,30] The NMF decomposition was applied to the obtained SERS maps, highlighting the SERS spectra corresponding to SERS tags subtracted from

https://doi.org/10.1021/acssensors.2c00610
ACS Sens. 2022, 7, 1747−1756

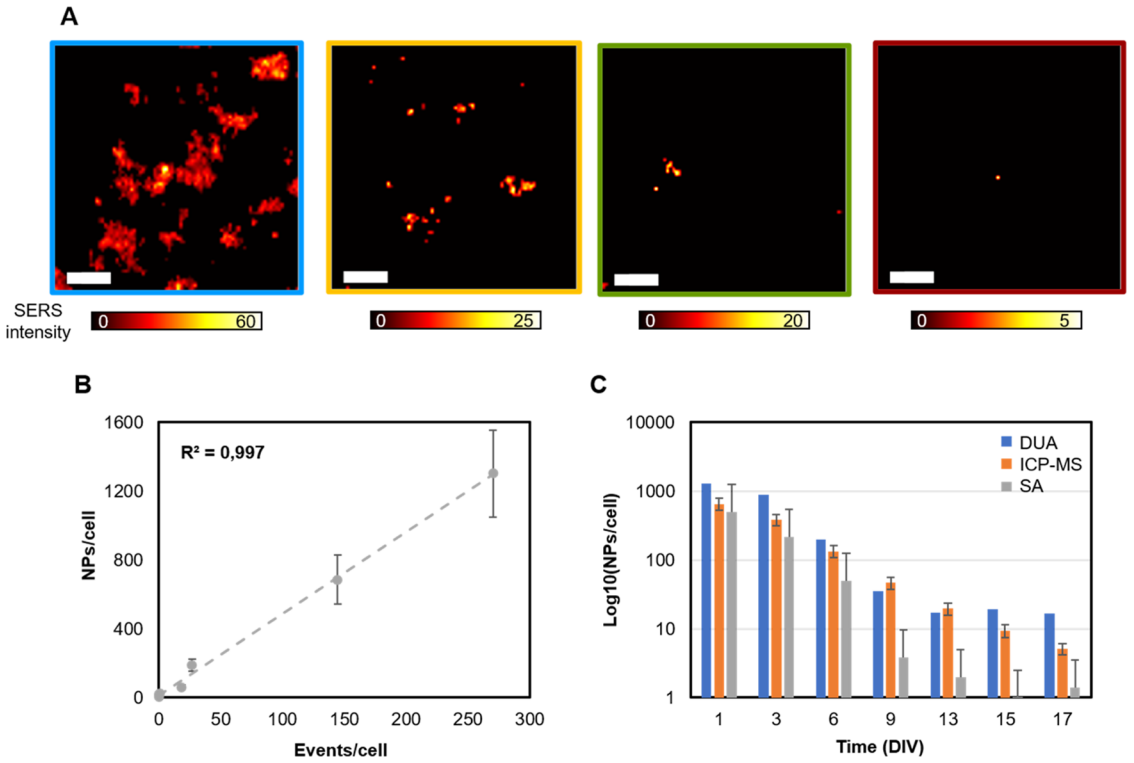

Figure 4. SERS analysis by DUA. (A) Single *z*-plane SERS maps, analyzed by the NMF algorithm, at four timepoints: 1 DIV, 6 DIV, 13 DIV, and 17 DIV. Scale bars = 15 μm. 4BPT-AuNS SERS tags were employed. (B) Linear relationship between the sum of selected spectra per cell at each timepoint and the amount of SERS tags calculated by ICP-MS. (C) Comparison between the three methodologies for the estimation of SERS tags inside cells.

the background noise. The initial maps were then analyzed considering a correlation level of $\rho \geq 0.75$ with respect to the reference identified in the previous step (see Figure S15). Indeed, this DUA approach was found to recover, with a high degree of co-localization, the SERS tag profile in 3D SERS images, obtained in complex biological media (Figures S16 and S17). Figure 4A shows the intensity of SERS tags, determined from a single z-plane at different DIVs, containing ca. 20 cells per map. The images were pretreated by the bicubic interpolation method[35] to improve visualization. We clearly observed a direct relationship between the number of SERS spectra selected per cell by the DUA algorithm (the events) and the number of NPs per cell obtained via ICP-MS, where only a few events were identified after DIV 13 (Figure 4B). These results were used to build a digital SERS tag calibration curve (dashed line in Figure 4B), which was subsequently applied to estimate the number of SERS tags inside cells that were incubated with a lower tag concentration (0.05 mM, or 1.9×10^9 NPs/mL). The estimated number of NPs per cell from both algorithms was compared with ICP-MS measurements in Figure 4C. As can be seen in Figure 4C, a better agreement with ICP-MS data was obtained when using the DUA at very low SERS tag concentrations, similar to the single-molecule quantification described in previous works.[30] In contrast, at high concentrations we found that numerous SERS tags could be found in the same imaging plane, illuminated by a laser spot of ~2.5 μm^2, which could explain some discrepancies observed between the digital counting of SERS tags and the evaluation from ICP-MS analysis (Figure S16).

CONCLUSIONS

We have developed algorithmic methods to quantify the intracellular amount of SERS tags, with the aim to characterize NP uptake and dilution into daughter cells *in vitro*. We introduced two multivariate approaches, one based on the supervised comparison with a reference spectrum by MLRA (supervised algorithm), and another based on an unsupervised method via NMF (digital SERS tags quantification protocol). Both protocols were validated by ICP-MS analysis, which is often used to quantify cell uptake of metal-containing NPs. Using the first approach, a close estimate of the number of NPs per cell was obtained from an analysis based on 3D SERS measurements of individual MCF7 live cells, with no undesired cytotoxicity from excessive laser exposure. On the other hand, the second unsupervised approach allowed us to extract the number of SERS tag events per cell, by applying an NMF blind procedure on the same raw SERS spectra. The number of events correlated well with ICP-MS results, so a calibration curve could be retrieved and then used to evaluate a second set of measurements. We were thus able to track the dilution of SERS tags to daughter cells for more than 2 weeks, ensuring the long-term labeling capacity of these biocompatible and optically sensitive labels. We additionally explored the decrease in SERS tag intensity over time, in terms of cellular division and exocytosis, identifying cellular division as the principal source of SERS tag dilution after 1 DIV. This is in agreement with other reports in which different experimental and algorithmic methods were used to study NP dilution into daughter cells.

The approaches presented for the quantification of SERS tags via SERS mapping open up the use of this methodology to

https://doi.org/10.1021/acssensors.2c00610
ACS Sens. 2022, 7, 1747−1756

study the interaction of SERS tags with live cells *in vitro* with minimal invasiveness, and to characterize parameters such as NP dwelling time, which may vary depending on the NPs and cell lines used. These findings are important to study increasingly complex 3D cellular systems through SERS imaging, with control over all parameters affecting the final image. In this case, the long dwelling time of SERS tags (over 2 weeks), coupled with their nontoxic nature and high multiplexing ability, offers an interesting opportunity to use them in 3D cell models, even at low concentrations.

MATERIALS AND METHODS

Chemicals. Tetrachloroauric acid trihydrate ($HAuCl_4 \cdot 3H_2O$, ≥99%), citric acid (≥99.5%), L-ascorbic acid (≥99%), silver nitrate ($AgNO_3$, ≥99%), hexadecyltrimethylammonium bromide (CTAB, ≥99%), O-[2-(3-mercaptopropionylamino)ethyl]-O′-methylpolyethylene glycol (PEG, MW 5000 g/mol), 4-biphenylthiol (4BPT, 97%), 2-naphthalenethiol (2NAT, 99%), poly(isobutylene-alt-maleic anhydride) (average MW ∼6000 g/mol), dodecylamine (98%), 1-decanol, tetrahydrofuran (THF, 99.85%, extra dry), chloroform ($CHCl_3$, ≥99.8%), and sodium hydroxide (NaOH, >97%) were purchased from Sigma-Aldrich. Hydrochloric acid solution (37 wt %) was purchased from Fisher Chemical. All chemicals were used without further purification. Milli-Q water (resistivity 18.2 MΩ·cm at 25 °C) was used in all experiments. All glassware was washed with aqua regia, rinsed with Milli-Q water, and dried prior to use. Dulbecco's modified Eagle's medium (DMEM), fetal bovine serum (FBS), and penicillin−streptomycin (PS) were purchased from Invitrogen. FBS and PS were used at 10 and 1%, respectively, to make complete DMEM (cDMEM). All cells were grown in cDMEM, and Trypsin-EDTA was used for cell passage.

NPs Synthesis. SERS tags, AuNSs and AuNRs coated with 4BPT and 2NAT, respectively, were synthesized and characterized as previously reported.[8] The final concentration of the SERS tags was $[Au^0]$ = 0.5 mM, corresponding to 1.9×10^{10} NPs/mL. With the exception of the first experiment (Figures 1A,B and S2), we employed 4BPT-coated AuNSs as SERS tag for this work. Although both SERS tags (4BPT-AuNS and 2NAT-AuNR) would be appropriate, higher SERS signal intensities were obtained when combining MCF7 cells with 4BPT-AuNS, compared to 2NAT-AuNR. This is in agreement with other unpublished data, in which we observed slight differences in SERS tag uptake between different cell types. Therefore, we recommend that, prior to any long-term SERS experiment, an initial screening of cell-SERS tags is carried out to determine the optimal combination.

NPs Characterization. TEM images were collected with a JEOL JEM-1400PLUS transmission electron microscope operating at 120 kV, using carbon-coated 400 square mesh copper grids. UV−vis optical extinction spectra were recorded using an Agilent 8453 UV−vis diode array spectrophotometer. Regarding SERS tag stability, no aggregation was observed during storage at 4 °C. Prior to application to cells, a brief sonication step is recommended to efficiently redisperse sedimented SERS tags.

Cell Preparation for SERS Imaging. For the quantification over time of NPs in epithelial breast cancer cells (MCF7, ATCC#HTB-22), every 3−4 days the following protocol was repeated to prepare samples for SERS imaging and quantification of NPs inside cells and in the supernatant by ICP-MS. MCF7 cells were seeded at 5.7×10^4 cells/cm^2 on glass-bottomed dishes of 3.5 cm^2 area (Ibidi) and incubated for 24 h. Then, DMEM cell media containing 10% fetal bovine serum (herein cDMEM) was replaced with NPs diluted in cDMEM, and cells were incubated for an additional 24 h to allow NP uptake. Subsequently, the sample was divided: first, cell media was collected to quantify NPs in the supernatant by ICP-MS. Then, the cells were detached, counted, and separated as follows: 5×10^4 cells were resuspended in PBS and used to measure NPs in cells by ICP-MS (see details below), and 7×10^4 cells were transferred to an in-house designed SERS imaging holder (details reported in Figure S18). Finally, 2×10^5 cells were re-seeded to continue the experiments on the following days. The SERS imaging holder was composed of a quartz slide and a polylactic acid (PLA) 3D printed cell culture adaptor, designed with Autodesk Inventor Software (Autodesk Inc., CA), and fabricated with an Ultimaker 2 printer. Prior to cell seeding, the holder was cleaned using ethanol, dried, and glued to the quartz slide, followed by sterilization by UV light. SERS measurements were performed 2 h after plating the cells to allow them to adhere to the substrate.

Cell Preparation for ICP-MS. Each 3−4 days, 2×10^5 MCF7 cells were centrifuged at 1200 rpm for 5 min. Two freeze−thaw cycles were performed to promote the cell lysis. Then, the cell pellet (50 μL) was diluted in aqua regia (450 μL) for digestion.

Cell Preparation for Viability Assay. MCF7 cells were seeded at 2.8×10^4 cells/cm^2 in a dish with an imaging grid of 500 μm repeat distance (Ibidi). Once adhered, the cells were irradiated with different laser powers using a SERS confocal microscope equipped with a 785 nm laser. After 24 h, cell viability was monitored using a live/dead cell assay (ab115347, Abcam). For each irradiated section of the grid, the percentage of dead cells was quantified and represented by the number of dead cells with respect to the area of live cells (Figure S6).

Cell Preparation for TEM Imaging. MCF7 cells were seeded at 2×10^5 cells/well in a 12-well plate and allowed to adhere. Media was replaced with SERS tags diluted to ca. 20 μM in cDMEM and left overnight. Nonendocytosed SERS tags were removed by washing, and the cells were dissociated from the well using Trypsin-EDTA. The cells were fixed with formaldehyde/glutaraldehyde in Sorensen's buffer followed by agarose embedding and OsO_4 fixation/staining. Samples were dehydrated in an ethanol series followed by transfer to acetone and Spurs resin embedding. Ultramicrotomed sections measuring 100 nm thick were imaged using a JEOL JEM-1400PLUS transmission electron microscope operating at 120 kV.

TEM Grid Preparation for Signal Estimation of Single SERS Tags. A 200-mesh copper-carbon film London finder grid for electron microscopy was treated by glow discharge to hydrophilize the surface and obtain a homogeneous spreading of the particles. After 10 min in vacuum (10^{-1} mbar), we applied a negative polarity with a coating current of 30 mA for 2.5 min. Immediately after, we drop-cast 3 μL of SERS tags at $[Au^0]$ = 0.5 mM (1.9×10^{10} NPs/mL) to let them dry in air.

SERS Imaging Specifications. *SERS Tags Supervised Counting Algorithm.* SERS measurements were performed with a Raman microscope (inVia Reflex, Renishaw, Wotton-under-Edge, U.K.) equipped with a −60 °C Peltier-cooled front-illuminated CCD detector (1024 × 512 pixel^2 chip), using a 785 nm laser excitation source (maximum output 270 mW) and a 1200 lines/mm diffraction grating. SERS maps were recorded in static mode (center of scattered wavenumber 1450 cm^{-1}) using a 40× dip-in water immersion objective (numerical aperture, NA = 0.8; Nikon Corporation, Tokyo, Japan). For Figure 1, an area of 400 × 400 μm^2 was imaged with a 0.8 s integration time, at a 1.57 mW laser power (equivalent to a laser power density of 0.02 mW μm^{-2}) and a step size of 10 μm.

Phototoxicity. SERS measurements were performed with a confocal Raman microscope (Alpha300R WITec GmbH, Ulm, Germany) equipped with a −60 °C Peltier-cooled back-illuminated deep-depletion CCD detector (1024 × 128 pixel^2 chip), using a 785 nm laser excitation source (maximum output 83 mW) and a 300 lines/mm diffraction grating. The center of scattered wavenumber was set to 1450 cm^{-1}, and the signal was recorded using a 20× dip-in water immersion objective (NA = 0.5; Zeiss, Jena, Germany). The following settings were used in the figures as indicated. In all cases, the laser power density was calculated by P/A, where P is the laser power measured at surface (Si photodiode sensor, Ophir, Israel) through the corresponding objective and A is the illuminated area of the focused laser beam onto a silicon wafer measured from the video camera image. An area of 150 × 115 μm^2 was scanned, with a step size of 5 μm and an integration time of 0.02 s, increasing the laser power from 3 to 20 mW (corresponding power densities 1−6.4 mW μm^{-2}) (Figure S5). Two layers of 500 × 500 μm^2 area, at a 5 μm distance between each other, were scanned with different integration times

https://doi.org/10.1021/acssensors.2c00610
ACS Sens. 2022, 7, 1747−1756

(0.02 and 0.05 s) and laser powers (30 and 80 mW, equivalent to 9.6 and 25.6 mW μm^{-2}, respectively), and a 10 μm step size. Each map took ~6 min to be completed (Figure S6). Areas of ca. 60 × 80 μm^2 were scanned with a 5 mW laser power (equivalent to 1.6 mW μm^{-2}), a 0.02 s integration time, and a 5 μm step size (Figure 2A). Two layers of 500 × 500 μm^2 area at a 5 μm distance between each other were scanned with a 5 mW laser power (equivalent to 1.6 mW μm^{-2}), a 0.02 s integration time, and a 10 μm step size (Figure 2B). An area of 500 × 500 μm^2 was scanned with a 5 mW laser power (equivalent to 1.6 mW μm^{-2}), a 0.02 s integration time, and two different step sizes of 5 and 1 μm, as explained in Figure S7.

3D SERS Tags Supervised Counting Algorithm. SERS measurements were performed with a confocal Raman microscope (Alpha300R, WITec GmbH, Ulm, Germany) equipped with a −60 °C Peltier-cooled CCD detector (1024 × 128 $pixel^2$ chip), using a 785 nm laser excitation source (maximum output 83 mW) and a 300 lines/mm diffraction grating. The center of scattered wavenumber was set to 1450 cm^{-1}, and the signal was recorded using a 20× dip-in water immersion objective (NA = 0.5; Zeiss, Jena, Germany). For each DIV, two to three volumetric areas (average dimensions 84 × 84 × 25 μm^3, which contained around 10−20 cells) were imaged with a 5 mW laser power (equivalent to 1.6 mW μm^{-2}), a 0.02 s integration time, and step sizes of 1 μm in x and y, and 4 μm in z (Figures 3 and S12). An area of ca. 84 × 84 μm^2 was imaged with a 0.02 s integration time, a 1 μm step size, and two different laser powers (5 and 80 mW, equivalent to 1.6 and 25.6 mW μm^{-2}, respectively), as explained in Figure S13.

SERS Data Analysis. Data obtained with the Renishaw Raman microscope were first analyzed using the WiRE4.4 software (Renishaw, Wotton-under Edge, U.K.) to correct the baseline in the spectra (i.e., intelligent 11th polynomial order) and eliminate cosmic rays. Data obtained from the confocal Raman microscope Alpha300R were analyzed with the ProjectFIVE(+) software (WITec GmbH, Ulm, Germany) software, to correct the baseline (shape subtraction, furnished by the program) and eliminate cosmic rays.

Supervised Algorithm (SA). The spectra in 2D SERS mappings were analyzed by multiple linear regression (MLR) analysis (Regress function in Matlab),[25−27] which considers the full spectrum to assign a percentage of the presence of references, which are the typical fingerprints of SERS tags. This procedure assigns to each spectrum a so-called b value, one for each chosen reference, plus one b value for the background. It also provides a statistical p value for each assignment, which indicates the reliability of the analysis itself. Thus, it was possible to select only those points whose spectra had a certain percentage of similarity with the references: the first applied filter was on p values (i.e., p values <0.05), neglecting those points that could be not well assigned by the analysis; then, the second filter was applied to the b values, selecting only those higher than a second threshold called β, which was defined by the data features (here, b values > β = 6). In this way, we obtained a new 2D mapping containing only the spectra corresponding to the selected labels.

Non-Negative Matrix Factorization (NMF) Algorithm. The non-negative matrix factorization with alternative least squares algorithm was used to decompose 2D/3D SERS imaging data sets.[28] The NMF algorithm is an unsupervised method, so no prior information or reference spectra were needed. Therefore, we informed the number of factors using a second method, such as the singular value decomposition (SVD) to estimate the number of factors, and then the NMF algorithm was randomly initialized. Satisfactory NMF models were built with two factors, where low error (0.06) and high percentage of explained variance (ca. 100%) were estimated (see ref 29 for more details).

SA Applied to 3D Images. In the case of the 3D sum, the SA was applied to all of the layers of the scanned volume in a certain region and then the selected spectra were summed together. The cells were counted from the optical image, and then the previous sum was divided by this number, obtaining the average SERS intensity per cell. The number of SERS tags per cell was estimated by dividing the average SERS signal per cell by the signal of a single SERS tag, obtained from the analysis of the SERS tags deposited onto a TEM grid. In Figure S10C, the median value is reported with a red bar, while 25% and 75% are represented by a gray area and used to calculate the error on the number of NP per cell.

Digital SERS Tags Quantification Protocol (DUA). For the digital SERS tags approach, we used the recovered SERS tags profile from the NMF method to pick SERS tag spectra in 3D SERS imaging with a correlation level of the Pearson's linear correlation coefficient of $\rho \geq 0.75$. Next, we built a digital SERS tags calibration curve[30] with the number of events versus the number of SERS tags estimated by ICP-MS. However, rather than selecting the spectra within a given threshold by their similarities, we could effectively eliminate the background (see Figures S15 and S17).

■ ASSOCIATED CONTENT

Supporting Information

The Supporting Information is available free of charge at https://pubs.acs.org/doi/10.1021/acssensors.2c00610.

Simulation of 2D SERS mapping with SERS tag; ICP-MS study of low SERS tags labeling concentrations; additional studies of SERS tags toxicity under laser irradiation; TEM images of SERS tag uptake, redefinition of analysis parameters; individual SERS tag signal calibration in cellular measurements setup; estimation of the number of NPs in 3D live cells with SA; estimation of the number of NPs in 3D live cells with SA for the second gold concentration ([Au^0] = 0.05 mM or equivalently 1.9 × 10^9 NPs/mL); methods to improve NPs detection at low concentrations; additional information regarding DUA for quantification of SERS tags; and workflow for algorithm choice (PDF)

■ AUTHOR INFORMATION

Corresponding Authors

Dorleta Jimenez de Aberasturi − *CIC biomaGUNE, Basque Research and Technology Alliance (BRTA), 20014 Donostia-San Sebastián, Spain; Centro de Investigación Biomédica en Red, Bioingeniería, Biomateriales, y Nanomedicina (CIBER-BBN), 20014 Donostia-San Sebastián, Spain; Ikerbasque, Basque Foundation for Science, 48009 Bilbao, Spain;* orcid.org/0000-0001-5009-3557; Email: djimenezdeaberasturi@cicbiomagune.es

Luis M. Liz-Marzán − *CIC biomaGUNE, Basque Research and Technology Alliance (BRTA), 20014 Donostia-San Sebastián, Spain; Centro de Investigación Biomédica en Red, Bioingeniería, Biomateriales, y Nanomedicina (CIBER-BBN), 20014 Donostia-San Sebastián, Spain; Ikerbasque, Basque Foundation for Science, 48009 Bilbao, Spain;* orcid.org/0000-0002-6647-1353; Email: llizmarzan@cicbiomagune.es

Authors

Elisa Lenzi − *CIC biomaGUNE, Basque Research and Technology Alliance (BRTA), 20014 Donostia-San Sebastián, Spain; Centro de Investigación Biomédica en Red, Bioingeniería, Biomateriales, y Nanomedicina (CIBER-BBN), 20014 Donostia-San Sebastián, Spain*

Malou Henriksen-Lacey − *CIC biomaGUNE, Basque Research and Technology Alliance (BRTA), 20014 Donostia-San Sebastián, Spain; Centro de Investigación Biomédica en Red, Bioingeniería, Biomateriales, y Nanomedicina (CIBER-BBN), 20014 Donostia-San Sebastián, Spain*

Beatriz Molina − *CIC biomaGUNE, Basque Research and Technology Alliance (BRTA), 20014 Donostia-San*

https://doi.org/10.1021/acssensors.2c00610
ACS Sens. 2022, 7, 1747−1756

Sebastián, Spain; Present Address: Biobide Spain, Paseo Mikeletegi 56, Bajo, 20009 Donostia-San Sebastián, Spain

Judith Langer − *CIC biomaGUNE, Basque Research and Technology Alliance (BRTA), 20014 Donostia-San Sebastián, Spain; Centro de Investigación Biomédica en Red, Bioingeniería, Biomateriales, y Nanomedicina (CIBER-BBN), 20014 Donostia-San Sebastián, Spain;* orcid.org/0000-0003-3527-5728

Carlos D. L. de Albuquerque − *CIC biomaGUNE, Basque Research and Technology Alliance (BRTA), 20014 Donostia-San Sebastián, Spain; Centro de Investigación Biomédica en Red, Bioingeniería, Biomateriales, y Nanomedicina (CIBER-BBN), 20014 Donostia-San Sebastián, Spain;* orcid.org/0000-0002-7615-7325

Complete contact information is available at: https://pubs.acs.org/10.1021/acssensors.2c00610

Author Contributions

The manuscript was written through contributions of all authors. All authors have given approval to the final version of the manuscript. Dr. Lucio Litti is thanked for providing the simulations reported in Figure S1.

Funding

Financial support from the European Research Council (ERC Advanced Grant 787510, 4DbioSERS) and MCIN/AEI/10.13039/501100011033 through Grants # PID2019-108854RA-I00 and Maria de Maeztu Unit of Excellence No. MDM-2017-0720 is acknowledged.

Notes

The authors declare no competing financial interest.

■ ABBREVIATIONS

NP, nanoparticle; DIV, day *in vitro*; SERS, surface-enhanced Raman scattering; SA, supervised algorithm; DUA, digital unsupervised algorithm; NMF, non-negative matrix factorization; ICP-MS, inductively coupled plasma-mass spectrometry

■ REFERENCES

(1) Sreejith, S.; Huong, T. T. M.; Borah, P.; Zhao, Y. Organic−Inorganic Nanohybrids for Fluorescence, Photoacoustic and Raman Bioimaging. *Sci. Bull.* **2015**, *60*, 665−678.

(2) Langer, J.; Jiménez de Aberasturi, D.; Aizpurua, J.; Alvarez-Puebla, R. A.; Auguié, B.; Baumberg, J. J.; Bazan, G. C.; Bell, S. E. J.; Boisen, A.; Brolo, A. G.; et al. Present and Future of Surface-Enhanced Raman Scattering. *ACS Nano* **2020**, *14*, 28−117.

(3) Smith, B. R.; Gambhir, S. S. Nanomaterials for In Vivo Imaging. *Chem. Rev.* **2017**, *117*, 901−986.

(4) Lin, L.; Bi, X.; Gu, Y.; Wang, F.; Ye, J. Surface-Enhanced Raman Scattering Nanotags for Bioimaging. *J. Appl. Phys.* **2021**, *129*, No. 191101.

(5) Pallaoro, A.; Braun, G. B.; Moskovits, M. Biotags Based on Surface-Enhanced Raman Can Be as Bright as Fluorescence Tags. *Nano Lett.* **2015**, *15*, 6745−6750.

(6) Lenzi, E.; Jiménez de Aberasturi, D.; Liz-Marzán, L. M. Surface-Enhanced Raman Scattering Tags for Three-Dimensional Bioimaging and Biomarker Detection. *ACS Sens.* **2019**, *4*, 1126−1137.

(7) Reguera, J.; Langer, J.; Jiménez De Aberasturi, D.; Liz-Marzán, L. M. Anisotropic Metal Nanoparticles for Surface Enhanced Raman Scattering. *Chem. Soc. Rev.* **2017**, *46*, 3866−3885.

(8) Jiménez de Aberasturi, D.; Henriksen-Lacey, M.; Litti, L.; Langer, J.; Liz-Marzán, L. M. Using SERS Tags to Image the Three-Dimensional Structure of Complex Cell Models. *Adv. Funct. Mater.* **2020**, *30*, No. 1909655.

(9) García-Astrain, C.; Lenzi, E.; Jiménez de Aberasturi, D.; Henriksen-Lacey, M.; Binelli, M. R.; Liz-Marzán, L. M. 3D-Printed Biocompatible Scaffolds with Built-In Nanoplasmonic Sensors. *Adv. Funct. Mater.* **2020**, *30*, No. 2005407.

(10) Zhang, Y.; Jiménez de Aberasturi, D.; Henriksen-Lacey, M.; Langer, J.; Liz-Marzán, L. M. Live-Cell Surface-Enhanced Raman Spectroscopy Imaging of Intracellular PH: From Two Dimensions to Three Dimensions. *ACS Sens.* **2020**, *5*, 3194−3206.

(11) Wang, Z.; Zong, S.; Wu, L.; Zhu, D.; Cui, Y. SERS-Activated Platforms for Immunoassay: Probes, Encoding Methods, and Applications. *Chem. Rev.* **2017**, *117*, 7910−7963.

(12) Plou, J.; García, I.; Charconnet, M.; Astobiza, I.; García-Astrain, C.; Matricardi, C.; Mihi, A.; Carracedo, A.; Liz-Marzán, L. M. Multiplex SERS Detection of Metabolic Alterations in Tumor Extracellular Media. *Adv. Funct. Mater.* **2020**, *30*, No. 1910335.

(13) Lenzi, E.; Jiménez de Aberasturi, D.; Henriksen-Lacey, M.; Piñeiro, P.; Muniz, A. J.; Lahann, J.; Liz-Marzán, L. M. SERS and Fluorescence-Active Multimodal Tessellated Scaffolds for Three-Dimensional Bioimaging. *ACS Appl. Mater. Interfaces* **2022**, *14*, 20708−20719.

(14) Jiménez de Aberasturi, D.; Serrano-Montes, A. B.; Langer, J.; Henriksen-Lacey, M.; Parak, W. J.; Liz-Marzán, L. M. Surface Enhanced Raman Scattering Encoded Gold Nanostars for Multiplexed Cell Discrimination. *Chem. Mater.* **2016**, *28*, 6779−6790.

(15) Laing, S.; Gracie, K.; Faulds, K. Multiplex in Vitro Detection Using SERS. *Chem. Soc. Rev.* **2016**, *45*, 1901−1918.

(16) Summers, H. D.; Rees, P.; Holton, M. D.; Rowan Brown, M.; Chappell, S. C.; Smith, P. J.; Errington, R. J. Statistical Analysis of Nanoparticle Dosing in a Dynamic Cellular System. *Nat. Nanotechnol.* **2011**, *6*, 170−174.

(17) Rees, P.; Wills, J. W.; Brown, M. R.; Barnes, C. M.; Summers, H. D. The Origin of Heterogeneous Nanoparticle Uptake by Cells. *Nat. Commun.* **2019**, *10*, No. 2341.

(18) Kim, J. A.; Aberg, C.; Salvati, A.; Dawson, K. A. Role of Cell Cycle on the Cellular Uptake and Dilution of Nanoparticles in a Cell Population. *Nat. Nanotechnol.* **2012**, *7*, 62−68.

(19) Ha, S. W.; Camalier, C. E.; Weitzmann, M. N.; Beck, G. R.; Lee, J. K. Long-Term Monitoring of the Physicochemical Properties of Silica-Based Nanoparticles on the Rate of Endocytosis and Exocytosis and Consequences of Cell Division. *Soft Mater.* **2013**, *11*, 195−203.

(20) Bourquin, J.; Septiadi, D.; Vanhecke, D.; Balog, S.; Steinmetz, L.; Spuch-Calvar, M.; Taladriz-Blanco, P.; Petri-Fink, A.; Rothen-Rutishauser, B. Reduction of Nanoparticle Load in Cells by Mitosis but Not Exocytosis. *ACS Nano* **2019**, *13*, 7759−7770.

(21) Xiong, R.; Joris, F.; Liang, S.; De Rycke, R.; Lippens, S.; Demeester, J.; Skirtach, A.; Raemdonck, K.; Himmelreich, U.; De Smedt, S. C.; Braeckmans, K. Cytosolic Delivery of Nanolabels Prevents Their Asymmetric Inheritance and Enables Extended Quantitative in Vivo Cell Imaging. *Nano Lett.* **2016**, *16*, 5975−5986.

(22) Drasler, B.; Vanhecke, D.; Rodriguez-Lorenzo, L.; Petri-Fink, A.; Rothen-Rutishauser, B. Quantifying Nanoparticle Cellular Uptake: Which Method Is Best? *Nanomedicine* **2017**, *12*, 1095−1099.

(23) Lenzi, E.; Litti, L.; Jimenez de Aberasturi, D.; Henriksen-Lacey, M.; Liz-Marzán, L. M. SERSTEM: An App for the Statistical Analysis of Correlative SERS and TEM Imaging and Evaluation of SERS Tags Performance. *J. Raman Spectrosc.* **2021**, *52*, 355−365.

(24) De Albuquerque, C. D. L.; Schultz, Z. D. Super-Resolution Surface-Enhanced Raman Scattering Imaging of Single Particles in Cells. *Anal. Chem.* **2020**, *92*, 9389−9398.

(25) Brereton, R. G. Evolutionary Signals. In *Chemometrics*, John Wiley & Sons, Ltd., 2003; pp 339−407.

(26) Zhang, Y.; Wang, Z.; Wu, L.; Zong, S.; Yun, B.; Cui, Y. Combining Multiplex SERS Nanovectors and Multivariate Analysis for In Situ Profiling of Circulating Tumor Cell Phenotype Using a Microfluidic Chip. *Small* **2018**, *14*, No. 1704433.

(27) Pallaoro, A.; Hoonejani, M. R.; Braun, G. B.; Meinhart, C. D.; Moskovits, M. Rapid Identification by Surface-Enhanced Raman

Spectroscopy of Cancer Cells at Low Concentrations Flowing in a Microfluidic Channel. *ACS Nano* **2015**, *9*, 4328−4336.
(28) Lee, D. D.; Seung, H. S. Learning the Parts of Objects by Non-Negative Matrix Factorization. *Nature* **1999**, *401*, 788−791.
(29) Albuquerque, C. D.; Poppi, R. J. Detection of Malathion in Food Peels by Surface-Enhanced Raman Imaging Spectroscopy and Multivariate Curve Resolution. *Anal. Chim. Acta* **2015**, *879*, 24−33.
(30) De Albuquerque, C. D. L.; Sobral-Filho, R. G.; Poppi, R. J.; Brolo, A. G. Digital Protocol for Chemical Analysis at Ultralow Concentrations by Surface-Enhanced Raman Scattering. *Anal. Chem.* **2018**, *90*, 1248−1254.
(31) Furuya, Y.; Kohno, N.; Fujiwara, Y.; Saitoh, Y. Mechanisms of Estrogen Action on the Proliferation of MCF-7 Human Breast Cancer Cells in an Improved Culture Medium. *Cancer Res.* **1989**, *49*, 6670−6674.
(32) Panet, E.; Mashriki, T.; Lahmi, R.; Jacob, A.; Ozer, E.; Vecsler, M.; Lazar, I.; Tzur, A. The Interface of Nanoparticles with Proliferating Mammalian Cells. *Nat. Nanotechnol.* **2017**, *12*, 598−600.
(33) Feliu, N.; Sun, X.; Alvarez Puebla, R. A.; Parak, W. J. Quantitative Particle-Cell Interaction: Some Basic Physicochemical Pitfalls. *Langmuir* **2017**, *33*, 6639−6646.
(34) Lijster, T.; Åberg, C. Asymmetry of Nanoparticle Inheritance upon Cell Division: Effect on the Coefficient of Variation. *PLoS One* **2020**, *15*, No. e0242547.
(35) Keys, R. G. Cubic Convolution Interpolation for Digital Image Processing. *IEEE Trans. Acoust., Speech, Signal Process.* **1981**, *29*, 1153−1160.

https://doi.org/10.1021/acssensors.2c00610
ACS Sens. 2022, 7, 1747−1756